RSC Advances

PAPER

View Article Online
View Journal | View Issue

Cite this: *RSC Adv.*, 2025, **15**, 11409

A DFT study for hydrogen storage application on pristine magnesium dicarbide (MgC_2) monolayer

Irfan Ahmed,[a] Ukkasha Iqrar,[a] Ashir Saeed,[a] Rajeh Alotaibi,[b] Syed Mansoor Ali,[c] Maida Anwar[d] and Muhammad Isa Khan *[a]

Received 20th January 2025
Accepted 10th March 2025

DOI: 10.1039/d5ra00486a

rsc.li/rsc-advances

The hydrogen storage potential of pure MgC_2 was systematically investigated using density functional theory (DFT) calculations. The phonon dispersion and *ab initio* molecular dynamics (AIMD) simulations confirmed the dynamic and structural stability of MgC_2, reinforcing its suitability as a promising hydrogen storage material. The electronic structure analysis revealed that pure MgC_2 exhibits semiconducting behavior with a band gap of 0.25 eV, and transforms into a metallic state upon hydrogen adsorption. Hydrogen molecules were adsorbed onto the MgC_2 surface *via* physisorption, with an average adsorption energy of 0.286 eV, indicating moderate binding strength suitable for reversible hydrogen storage. Hirshfeld charge analysis demonstrated that MgC_2 transfers 0.041 e, 0.139 e, and 0.259 e to 1, 4, and 8 hydrogen molecules, respectively, highlighting charge redistribution upon adsorption. The calculated hydrogen storage capacity of 2.05% suggests a feasible adsorption mechanism. Additionally, AIMD simulations at 400 K confirmed that hydrogen adsorption does not induce significant distortions in the MgC_2 framework, further validating its thermal and mechanical stability. These findings underscore the potential of MgC_2 as an efficient hydrogen storage material for sustainable energy applications, offering a promising pathway for the development of next-generation clean energy technologies.

1. Introduction

One of the main and most efficient ways to address the enormous rise in energy consumption and environmental protection is the development of clean, sustainable energy sources like wind, solar, and hydrogen.[1–4] However, since hydrogen is not readily available in nature, it must be stored for use in transportation, as well as other mobile and stationary applications.[5,6] There are two types of hydrogen storage technologies: physical-based and material-based. The first category consists of currently in-use technologies that require specialized, big-volume containers to store hydrogen as compressed gas, cold/cryocompressed gas, and liquid.[7] The second method involves chemical reactions within materials at the atomic or molecular level. It is still quite difficult to find a substance that can safely, effectively, and affordably store hydrogen for real-world applications.[8,9] Recently, advancements in hydrogen storage technology have made it possible to store a substantial amount of hydrogen fuel safely, which has tremendously benefited the development of cars that run on hydrogen. Over the years, many efforts have been made to produce pure hydrogen (H_2) without harming the environment. According to the standards of the U.S. Department of Energy (DOE), a material used for hydrogen storage must have a storage gravimetric density of more than 5.5 wt%.[10]

In recent years, there has been enormous interest in nanostructured materials to store hydrogen by an adsorption mechanism.[11,12] These factors have led to the proposal of many materials, including MgH_2, $Mg(BH_4)_2$, and $LiBH_4$, for the solid-state storage of hydrogen. Despite having a high gravimetric density of hydrogen, these materials exhibit significant dissociation temperatures and thermodynamic stability.[13,14] The hydrogen storage capacity and recovery efficiency of carbon-based nanomaterials, such as graphene, are significantly influenced by lithium- and sodium-decorated inorganic graphenylene.

Although surface adsorption of H_2 is inefficient for hydrogen release, it is appropriate for improving the quantity of storage. Additionally, to keep the reservoir pressure high once H_2 has been retrieved, an absorbent gas, such as N_2, CH_4, or CO_2, is required. This leads to competitive adsorption between H_2 and the cushion gas, significantly affecting H_2 recovery and purification in the recovered fluids.[15] Consequently, none of them is a good option. On the other hand, magnesium hydride (MgH_2) has attracted significant attention due to its high volumetric

[a]*Department of Physics, Rahim Yar Khan Campus, The Islamia University of Bahawalpur, Bahawalpur, Pakistan. E-mail: irfanjamm315@gmail.com; ashir.saeed@iub.edu.pk; ui939msc@gmail.com; muhammad.isa@iub.edu.pk*

[b]*Department of Chemistry, College of Science, King Saud University, P. O. BOX 145111, Riyadh, Saudi Arabia. E-mail: raalotaibi@ksu.edu.sa*

[c]*Department of Physics and Astronomy, College of Science, King Saud University, P. O. BOX 2455, Riyadh 11451, Saudi Arabia. E-mail: symali@ksu.edu.sa*

[d]*Department of Physics and Astronomy "Galileo Galilei", University of Padua, Via VIII febbraio 2, 35122 Padua, Italy. E-mail: maidaanwar2021@gmail.com*

capacity (110 g L^{-1}) and gravimetric density (7.6 wt%), non-toxicity, good reversibility, and vast natural reserves. Furthermore, when supplying mixed gases free of harmful components, materials like MgH_2 show enormous potential for hydrogen filtration and selective storage.[16,17] Qin *et al.* conducted first-principles calculations to investigate the structural, mechanical, electronic, dynamic, thermodynamic, optical, and hydrogen storage properties of $XMoH_3$ (X = Na, K, Rb, Cs). Their findings confirm the thermodynamic, mechanical, and dynamic stability of these perovskites based on formation energy, elastic constants, and phonon spectra.[18]

Recent investigations have explored the potential of newly proposed 2D MXene materials, including Sc_2C, Cr_2C, Ti_2C, Ti_2N, and V_2C for hydrogen storage applications. Liu *et al.* investigated the use of V_2C (vanadium carbide) and Ti_3C_2 (titanium carbide) MXenes in combination to improve the capacity of MgH_2 to absorb and desorb hydrogen. By incorporating $2V_2C/Ti_3C_2$, the activation energy for the hydrogen release process of magnesium hydride (MgH_2) was successfully reduced by 36%, resulting in a reversible capacity of 6.3%.[19]

The SiB_2 monolayer, recognized for its lightweight nature, high carrier mobility, and exceptional stability, holds significant potential as an electrode material. Its structure is similar to that of MgB_2, which has been extensively studied.[20,21] The MgB_2 has been investigated for applications such as hydrogen storage and alkali metal ion batteries. The hydrogenation of bulk MgB_2 requires high pressure (90–100 MPa) and temperature (390–400 °C) and is time-intensive. Li *et al.* studied nanoscale MgB_2 hydrogenation *via* mechanical milling, though the reaction pathway and intermediate states remain unclear.[22] Theoretical studies suggest that Li decoration can enhance hydrogen storage capacity to 7.26 wt%,[23] while Na and Li addition improves H_2 storage efficiency in C_2O by 13.08 wt%.[24] In our previous study, we employed DFT to investigate optimized structures, thermodynamic properties, and H_2 storage capacities of MgB_2. The results highlight a subtle charge transfer from Li/Na/K to the MgB_2 monolayer, enhancing its electropositive nature and improving electrostatic interactions with H_2 molecules. The maximum H_2 adsorption occurs with nine H_2 molecules for Li and eight H_2 molecules for Na and K. The corresponding adsorption energies range from −0.24 to −0.21 eV for Li, −0.22 to −0.20 eV for Na, and −0.25 to −0.20 eV for K.[25] Previously, we have investigated various 2D materials and transition metal chalcogenides (TMDs) for alkali and alkaline earth metal-ion batteries, focusing on their structural, adsorption, electronic properties, open-circuit voltage (OCV), theoretical capacity, and thermodynamic stability.[26–31]

From the above discussion, it is clear that a thorough analysis of pristine MgC_2's capacity to store hydrogen, taking van der Waals correction parameters into account, has not yet been carried out. This gap inspired us to conduct a DFT calculation from the ground up to examine the hydrogen-adsorbed MgC_2 system's electrical characteristics, binding/adsorption energies, and desorption temperatures.

2. Computational detail

The Amsterdam density functional (ADF-BAND) software was used in the DFT framework, and Slater Type Orbitals (STO) was primarily used to create molecular orbitals for every structure.[32] Based on the framework offered by the Perdew–Burke–Ernzerhof (PBE) functional, the generalized gradient approximation (GGA) was used throughout the study to compute the exchange-correlation energies required for structure optimization. Given that van der Waals forces are the main interaction forces between H_2 and the substrate material, we addressed the shortcomings of DFT by integrating the Grime semi-empirical correction technique (DFT-D3) throughout the calculations in handling dispersive interactions. Additionally, our method used double-zeta polarized (DZP) basis sets and excellent numerical quality, together with settings that permitted non-frozen cores.[33] For fully relaxed geometries, we impose strict requirements, with an energy optimization threshold of 10^{-5} eV. We maintained 10^{-3} Å as the step convergence criterion and 0.02 eV $Å^{-1}$ as the gradient convergence criterion. Hirshfeld charge analysis was used to probe the arrangement of electrical ions between the absorption setups and optimum substances.

The adsorption energy of hydrogen molecules on pure MgC_2 is calculated by following the formula.

$$E_{ads} = \frac{E_{MgC_2} + nE_{H_2} - E_{(MgC_2-nH_2)}}{n} \quad (1)$$

where E_{MgC_2} denotes the total energy of MgC_2, $E_{MgC_2} + nE_{H_2}$ denotes the energy of hydrogen adsorbed MgC_2, and n denotes the amount of hydrogen molecule, E_{H_2} is the energy of a single H_2 molecule.[34]

To determine hydrogen adsorption on the MgC_2 nanosheet, we calculated the binding energy (E_{BE}) of the H_2 molecule using the following relation[35]

$$E_{BE} = E_{MgC_2} + nE_{H_2} - E_{nH_2-MgC_2} \quad (2)$$

where, E_{MgC_2}, nE_{H_2}, n, and $E_{nH_2-MgC_2}$ are the total energies of pristine MgC_2 nanosheet, an isolated H_2 molecule, n is the number of H_2 molecules and MgC_2 nanosheet with adsorbed H_2 molecules, respectively.

To determine the gravimetric storage capacity, the following formula was used:

$$wt\% = \frac{n \times M_{H_2}}{n \times M_{H_2} + M_{MgC_2}} \times 100\% \quad (3)$$

where M_{H_2} is the molecular mass of the H_2 molecule, M_{MgC_2} molecular mass of the host MgC_2, n is the number of adsorbed H_2 molecules.

The desorption temperature (T_d) of hydrogen-adsorbed systems is crucial for practical applications. We used the Van't Hoff equation to analyze the desorption temperature.[35,36]

$$T_D = \frac{E_{ads}}{k_b} \times \left(\frac{\Delta S}{R} - \ln P\right)^{-1} \quad (4)$$

where k_b is Boltzmann constant (1.380×10^{-23} J K^{-1}), ΔS represents the difference for hydrogen entropy switching from gaseous to the liquid state (75.44 J mol^{-1} K^{-1}), R is the universal gas constant (8.314 J mol^{-1} K^{-1}), and equilibrium pressure is 1 atm.

The desorption energy (E_{des}) is calculated as follows:

$$E_{des} = E_{H_2} + E_{MgC_2+(n-1)H_2} - E_{MgC_2+nH_2} \quad (5)$$

where E_{des} and $E_{MgC_2+(n-1)H_2}$ are gradual desorption energy and net energy of MgC_2 with $(n-1)$ H_2 adsorption, respectively.

3. Results and discussion

3.1 Structural and electronic properties of MgC_2 monolayer

The relaxed crystal structure of the MgC_2 monolayer within the *P6mm* space group is shown in Fig. 1(a). We have previously computationally designed MgB_2 and analyzed its structural, electronic, and adsorption properties. This material was investigated for hydrogen storage applications after being decorated with alkali metals.[25] Similarly, the MgC_2 structure was designed computationally by replacing the B atoms in MgB_2 with C atoms. MgB_2 consists of two atomic layers and exhibits a geometry similar to that of BeB_2, HfB_2, TiB_2, FeB_2, and MgB_2 monolayers.[36–39]

The upper atomic layer, composed of C atoms, follows a honeycomb arrangement similar to graphene, and the lower atomic layer consists of Mg atoms positioned at the center of the C–C honeycomb. The optimized lattice parameters of MgC_2 are $a = b = 3.181$ Å, which are slightly larger than those of the BeB_2 monolayer ($a = b = 3.032$ Å) and MgB_2 ($a = b = 3.017$ Å). Additionally, the monolayer thickness of MgC_2 is 1.460 Å, significantly greater than that of BeB_2 (0.443 Å) and less than MgB_2 (1.683 Å). A comparison of the lattice parameters is provided in Table 1.

Table 1 Lattice parameters, bond length, and height of MgC_2 monolayer

	Lattice parameters (Å)	Bond length(Å)	Height (Å)
MgC_2(this work)	**3.181**	**2.14**	**1.46**
MgB_2	3.017	2.42	1.68
BeB_2	3.032	1.84	0.44
HfB_2	3.165	2.32	1.41
TiB_2	3.083	1.73	1.19

Fig. 1(b and c) illustrates the band structure and density of states (DOS) of MgC_2. The DOS results indicate that the material exhibits semiconducting behavior with a bandgap of 0.30 eV. The band structure indicates the direct bandgap of 0.3 eV at Γ point which is consistent with the DOS. The total DOS is mainly governed by the p-orbitals of carbon atoms, with only a minor contribution from the s-orbitals of magnesium atoms. Fig. 1(b)

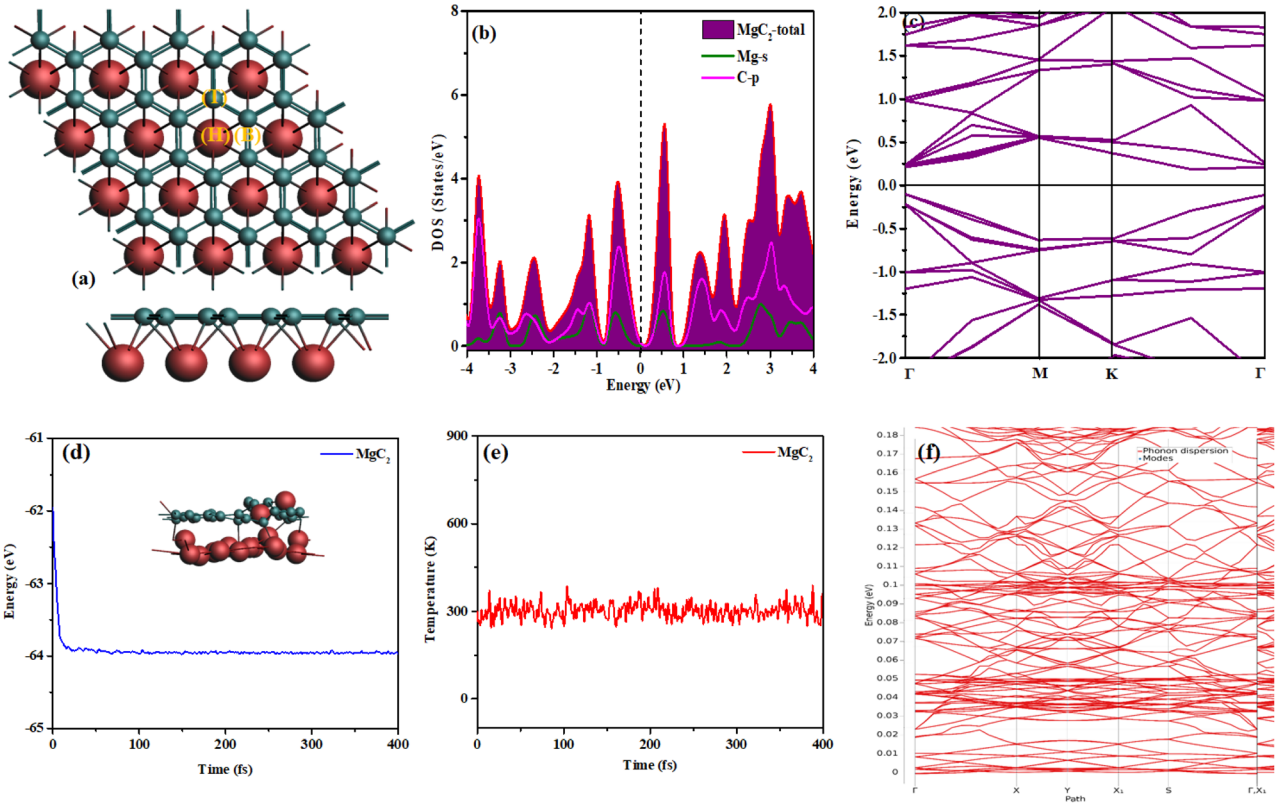

Fig. 1 Optimized structure of (a) MgC_2, (b) density of states (DOS), and (c) band structure (d) energy–time (e) temperature–time (f) phonon of MgC_2. Green-colored atoms represent boron, while maroon-colored atoms represent magnesium.

Table 2 Binding energy of MgC_2 at studied sites

Adsorption sites	TOP (T)	Bridge (B)	Hollow (H)
Binding energy (eV)	0.23	0.25	0.25

reveals that the s-orbital of Mg and the p-orbital of C overlap in the valence band.

MD calculations were conducted at 300 K for the pure MgC_2 monolayer. As observed in Fig. 1d and e, the energy graph peaks at −62 eV, while the temperature graph reaches a maximum value of 460 K. The continuous fluctuations in both graphs indicate the structural stability of MgC_2 at 300 K. The phonon calculations for the pure MgC_2 monolayer reveal no imaginary frequencies throughout the Brillouin zone, indicating its dynamic stability as shown in Fig. 1f. The absence of imaginary peaks in the phonon dispersion spectrum confirms that the structure remains stable under small perturbations and does not undergo spontaneous distortions or soft modes. This result validates the robustness of the material and supports its potential for practical applications.

3.2 Adsorption of hydrogen molecule on pristine MgC_2

This section examines the interaction of H_2 molecules with MgC_2, where a single H_2 molecule was placed at various distinct locations, as shown in Fig. 1(a). The hydrogen adsorption sites include (i) the hollow site of the hexagonal boron ring (H), (ii) the top of a boron atom (T), and (iii) the bridge site between two boron atoms (B). The structures were sequentially optimized by varying the adsorption sites. The binding energy was calculated using the formula in eqn (2), and the corresponding values for different sites are presented in Table 2.[35]

The binding energy estimates for these adsorption sites are presented in Table 2, and all values fall within the DOE criteria range (0.2–0.8 eV per H_2), making them suitable for hydrogen adsorption. The binding energy values for the H and B sites were found to be similar or higher. However, hydrogen initially placed at the B site migrated to the H site, indicating that the H site is more stable than the B site. Consequently, additional hydrogen molecules were sequentially adsorbed onto the H site, and their binding energies were calculated, as shown in Table 3.[25,40,41] The 5.73 Å is the ideal upward distance for a deposited H_2 molecule. In reference, the mean bond length of a free H_2 molecule is approximately 0.74 Å. An H_2 molecule adsorbed on the structure and caused a little increase in bond length to 0.75 Å.[42] The retention of H_2 molecular properties is indicated by the change in bond length that is seen throughout the procedure of adsorption and optimization. To determine the optimal adsorption site, adsorption energies were analyzed. Following structural optimization, the hexagonal hollow site emerged as the most favorable location for H_2 adsorption, with an average binding energy of 0.24 eV.[10,43]

3.3 Adsorption and electronic properties of H_2 molecule adsorbed on MgC_2

Based on the binding energy, it is concluded that the most favorable atom decoration occurs at the H site. Fig. 2 illustrates the optimized structures of hydrogenated MgC_2. Hydrogen molecules were sequentially adsorbed onto the H site, up to a total of $8H_2$, and their binding energy, adsorption energy, weight percentage, desorption energy, and desorption temperature were calculated, as detailed in Table 3.

Subsequently, each structure was optimized, and a vertical distance of 3.02 Å was determined to be optimal for the adsorbed H_2 molecule. It is discovered that the free H_2 molecule's bond length is 0.74 Å. The H–H bond length elongates to 0.78 Å when one H_2 molecule is added to the system. The H–H bond length in the $2H_2$–$8H_2$ molecule adsorption system is determined to be 0.78–0.80 Å. The H–H bond length determined throughout the adsorption and optimization procedures demonstrates that the molecule's structure remains intact.[42]

As shown in Fig. 3, the total and partial DOS were calculated for the Mg-s, C-p, H-s, and s orbitals of all metal elements to evaluate the system's electrochemical properties. Fig. 3(a) reveals that absorption of a single molecule of hydrogen transforms the behavior of MgC_2 from semiconducting to metallic, resulting in a zero bandgap. The p orbital of the C atom significantly contributes to the total DOS, while the s orbital of hydrogen exhibits overlapping peaks at −4.5 eV in the valence band, and hybridized peaks between 6–8 eV in the conduction band. Similarly, Fig. 3(b) demonstrates that after the adsorption of four hydrogen molecules, MgC_2 retains its metallic nature with a zero bandgap. The p orbital of the C atom remains the dominant contributor to total DOS, while the s orbital of hydrogen displays hybridized peaks within the ranges

Table 3 Binding, adsorption energy, weight percentage, and desorption temperature values

	Binding energy (eV)	Adsorption energy (eV per H_2)	Weight percent (%)	Desorption energy (eV)	Desorption temperature (K)
MgC_2–$1H_2$	0.25	0.290	0.26	0.29	370.52
MgC_2–$2H_2$	0.40	0.242	0.52	0.20	309.19
MgC_2–$3H_2$	0.62	0.234	0.77	0.21	298.97
MgC_2–$4H_2$	0.82	0.226	1.03	0.20	288.75
MgC_2–$5H_2$	1.03	0.223	1.29	0.21	284.92
MgC_2–$6H_2$	1.24	0.220	1.54	0.20	281.08
MgC_2–$7H_2$	1.44	0.218	1.80	0.20	278.53
MgC_2–$8H_2$	1.62	0.640	2.05	0.17	817.71

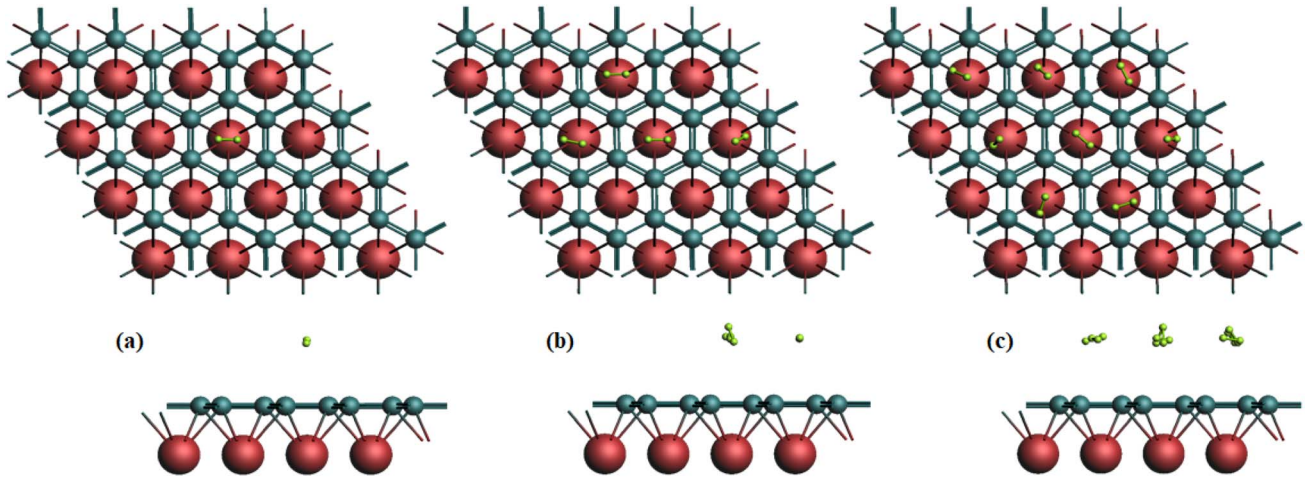

Fig. 2 Optimized structures of (a) $1H_2$- (b) $4H_2$- (c) $8H_2$-adsorbed MgC_2.

of −4 to −6 eV in the valence band and 6 to 8 eV in the conduction band.

In Fig. 3(c), the total DOS of MgC_2 after the adsorption of eight hydrogen molecules shows a reduction in the bandgap. The p orbital of the C atom remains the primary contributor to the total DOS, while the s orbital of hydrogen exhibits overlapping peaks at 7.1 eV in the conduction band and hybridized peaks within the ranges of −4 to −6 eV in the valence band and 6 to 8 eV in the conduction band. In summary, the adsorption between MgC_2 and hydrogen is primarily driven by the polarizing effect of the localized voltage generated by charged particles and their spatial recombination.

After the adsorption of hydrogen molecules onto the MgC_2 monolayer, charge analysis calculations were conducted. The results reveal that 1, 4, and 8 hydrogen molecules withdraw charges of 0.041 e, 0.139 e, and 0.259 e from the surface, respectively. For MgC_2, the typical hydrogen desorption temperature ranged from 370 K to 496 K for $1H_2$. As illustrated in Fig. 4, these values were derived from adsorption energies calculated within a pressure range of 1–10 atm.

Furthermore, three critical temperatures related to hydrogen desorption were determined: the maximum temperature at which desorption takes place (max-TD), the minimum temperature necessary to start hydrogen release (min-TD), and the average desorption temperature (Av-TD). In our study, the

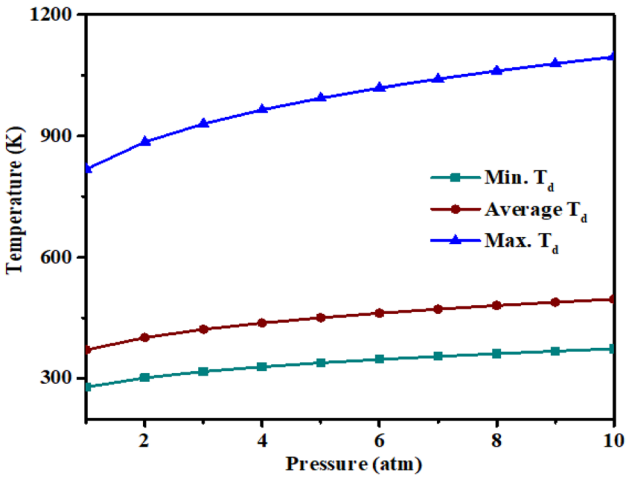

Fig. 4 Minimum, average, and maximum values for desorption temperature after hydrogen adsorption on MgC_2.

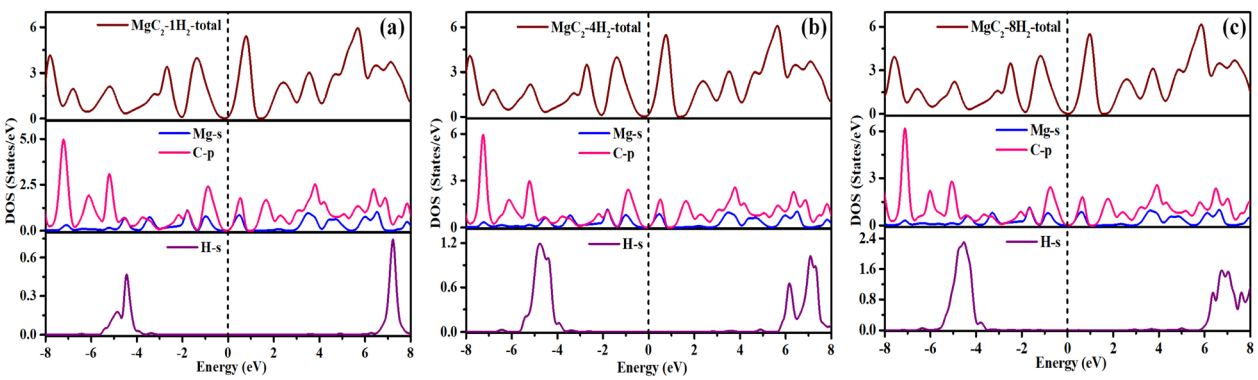

Fig. 3 DOS of (a) $1H_2$, (b) $4H_2$, (c) $8H_2$ adsorbed MgC_2.

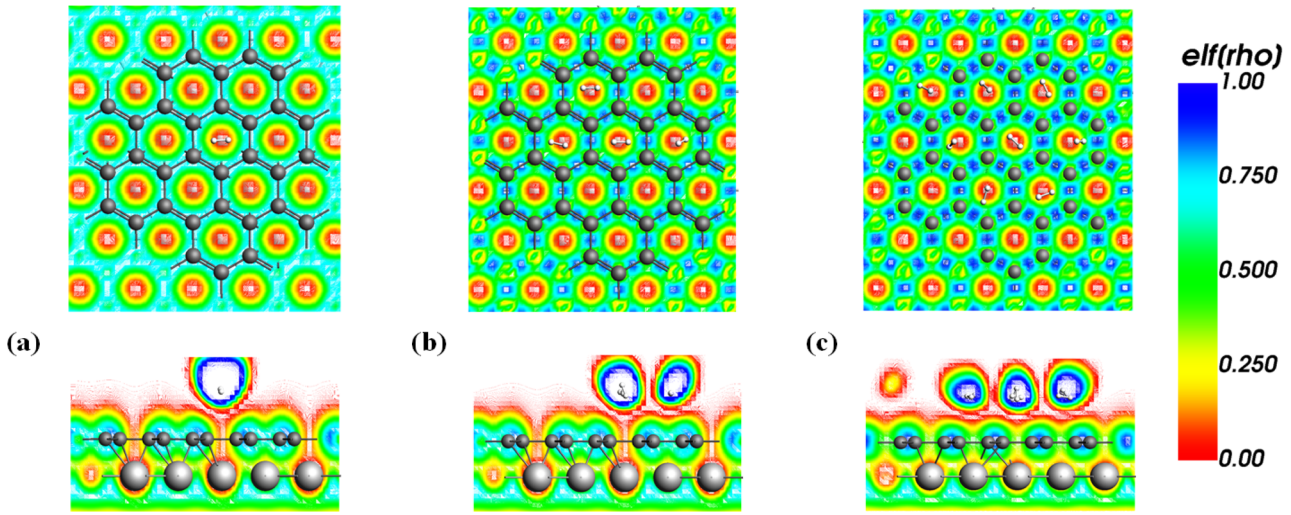

Fig. 5 (a) MgC_2–$1H_2$, (b) MgC_2–$4H_2$, (c) MgC_2–$8H_2$.

average desorption temperature of MgC_2 monolayers was calculated to range from 370 K to 496 K, indicating their suitability for fuel cell applications.[44]

3.4 Electron localization function (ELF)

The charge carrier density mechanism serves as a gauge of charge confinement and scattering and is connected to the kinetic energy density.[45,46] Its values range from 0.5 to 1.0, indicating areas where electrons are present and engaged in bonding or nonbonding interactions, including lone pairs, covalent bonds, or atomic shells. On the other hand, values between 0.0 and 0.5 show that there are small intermolecular interactions, and electrons are dispersed throughout the atomic shells.[47] The ELF map highlights regions of increased electron concentration and shows how charge carrier density changes on surfaces and adsorbents during complex creation.

As seen in Fig. 5(a) a value near 0.5 is indicated by green, indicating the presence of covalent bonds, and a large charge density is indicated by the increased red coloration in the MgC_2 layer after deposition of $1H_2$.[48] Following the uptake of four hydrogen molecules, Fig. 5(b) shows a striking color shift with an increase in green and a decrease in red and yellow, suggesting covalent electron sharing between the hydrogen molecules and the MgC_2 layer. The bright red hue represents a decrease in surface electrons, while the increasing green color and the presence of a light blue shade in Fig. 5(c) indicate charge transfer from the MgC_2 layer to the hydrogen molecules, with up to eight hydrogen molecules adsorbed.

3.5 *Ab initio* molecular dynamics (AIMD)

AIMD calculations were performed to assess the configurational stability of the system after hydrogen adsorption on MgC_2 at elevated temperatures such as 400 K. Simulations were conducted with a time step of 0.25 femtoseconds for a total duration of approximately 4.5 picoseconds at a temperature of 400 K. Fig. 6 presents the temperature and energy fluctuation graphs at 400 K.

As can be seen from Fig. 6(a1), the system attained higher energy values of −1706.5 eV when one hydrogen molecule was adsorbed on MgC_2. Fig. 6(a2) shows that the temperature peaks peaked at 5000 K. Based on Fig. 6(b1), it can be concluded that the system achieved higher energy values of −1855.9 eV when the eight hydrogen molecules were adsorbed on MgC_2. Fig. 6(b2) shows the temperature peaks around 4500 K. The steady fluctuations of the peaks indicate the stability of the MgC_2 sheet after hydrogen adsorption at 300 K.

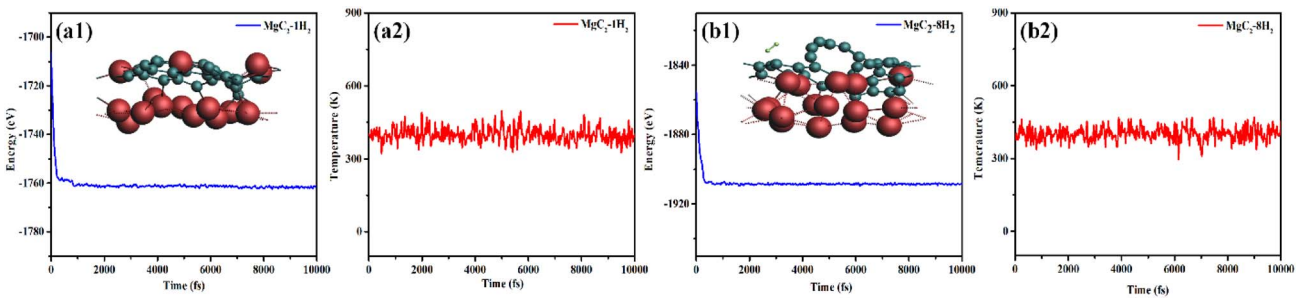

Fig. 6 Energy and temperature graph of (a1 and a2) MgC_2–$1H_2$ and (b1 and b2) MgC_2–$8H_2$.

4. Conclusion

In this study, the adsorption behavior of hydrogen on pure MgC_2 was systematically analyzed using density functional theory (DFT) and *Ab Initio* Molecular Dynamics (AIMD) simulations. The structural stability of MgC_2 was thoroughly evaluated using phonon dispersion calculations and AIMD simulations, confirming its robustness as a potential hydrogen storage material. MgC_2 demonstrates a gravimetric hydrogen capacity of 2.05 wt%, capable of adsorbing up to eight hydrogen molecules. The hydrogen changes the behavior of the pure MgC_2 to metallic. The average adsorption energy for MgC_2 was calculated to be 0.286 eV. Hirshfeld charge analysis revealed charge transfers of 0.041, 0.139, and 0.259 e to 1, 4, and 8 hydrogen molecules to the pure MgB_2 structures respectively. AIMD simulations confirmed that the pure MgC_2 structure remains stable without any distortions upon hydrogen adsorption at 400 K. The comprehensive analysis of structural, electronic, and adsorption properties, along with binding energy calculations, desorption temperature and energy assessments, charge density analysis, and electron localization function (ELF) mapping, all indicate that MgC_2 is a highly promising candidate for hydrogen storage applications. The strong interaction between MgC_2 and hydrogen molecules, coupled with favorable adsorption and desorption characteristics, suggests its potential for practical hydrogen storage solutions. These findings provide a theoretical foundation for further experimental validation and the development of MgC_2-based hydrogen storage materials.

Data availability

Data is available on request from the authors.

Conflicts of interest

There are no conflicts to declare.

Acknowledgements

The authors would like to extend their sincere appreciation to the Researcher supporting program at King Saud University, Riyadh, for funding this work under project number (RSPD2025R644).

References

1 Y. Yong, Q. Hou, X. Yuan, H. Cui, X. Li and X. Li, Ultrahigh capacity and reversible hydrogen storage media based on Li-decorated T-BN monolayers, *J. Energy Storage*, 2023, **72**, 108169.
2 S. R. Sinsel, R. L. Riemke and V. H. Hoffmann, Challenges and solution technologies for the integration of variable renewable energy sources—a review, *renewable energy*, 2020, **145**, 2271–2285.
3 S. E. Hosseini and M. A. Wahid, Hydrogen from solar energy, a clean energy carrier from a sustainable source of energy, *Int. J. Energy Res.*, 2020, **44**(6), 4110–4131.
4 J. O. Abe, A. Popoola, E. Ajenifuja and O. M. Popoola, Hydrogen energy, economy and storage: Review and recommendation, *Int. J. Hydrogen Energy*, 2019, **44**(29), 15072–15086.
5 P. Banerjee, B. Pathak, R. Ahuja and G. Das, First principles design of Li functionalized hydrogenated h-BN nanosheet for hydrogen storage, *Int. J. Hydrogen Energy*, 2016, **41**(32), 14437–14446.
6 M. Felderhoff, C. Weidenthaler, R. von Helmolt and U. Eberle, Hydrogen storage: the remaining scientific and technological challenges, *Phys. Chem. Chem. Phys.*, 2007, **9**(21), 2643–2653.
7 S. Niaz, T. Manzoor and A. H. Pandith, Hydrogen storage: Materials, methods and perspectives, *Renewable Sustainable Energy Rev.*, 2015, **50**, 457–469.
8 M. Jiang, J. Xu, P. Munroe, Z.-H. Xie and Z. Chen, Light metal decorated graphene-like Si2BN monolayers as hydrogen storage media: A DFT investigation, *Int. J. Hydrogen Energy*, 2024, **50**, 865–878.
9 Y. Zhu, L. Ouyang, H. Zhong, J. Liu, H. Wang, H. Shao, Z. Huang and M. Zhu, Closing the loop for hydrogen storage: facile regeneration of NaBH4 from its hydrolytic product, *Angew. Chem.*, 2020, **132**(22), 8701–8707.
10 X. Jin, P. Qi, H. Yang, Y. Zhang, J. Li and H. Chen, Enhanced hydrogen adsorption on Li-coated B12C6N6, *J. Chem. Phys.*, 2016, **145**(16), 164301.
11 A. Ahmed, S. Seth, J. Purewal, A. G. Wong-Foy, M. Veenstra, A. J. Matzger and D. J. Siegel, Exceptional hydrogen storage achieved by screening nearly half a million metal-organic frameworks, *Nat. Commun.*, 2019, **10**(1), 1568.
12 Y. Fu, Z. Yu, S. Guo, Y. Li, Q. Peng, L. Zhang, S. Wu and S. Han, Catalytic effect of bamboo-like carbon nanotubes loaded with NiFe nanoparticles on hydrogen storage properties of MgH2, *Chem. Eng. J.*, 2023, **458**, 141337.
13 M. Lakhal, M. Bhihi, A. Benyoussef, A. El Kenz, M. Loulidi and S. Naji, The hydrogen ab/desorption kinetic properties of doped magnesium hydride MgH2 systems by first principles calculations and kinetic Monte Carlo simulations, *Int. J. Hydrogen Energy*, 2015, **40**(18), 6137–6144.
14 S.-i. Orimo, Y. Nakamori, J. R. Eliseo, A. Züttel and C. M. Jensen, Complex hydrides for hydrogen storage, *Chem. Rev.*, 2007, **107**(10), 4111–4132.
15 A. Ozarslan, Large-scale hydrogen energy storage in salt caverns, *Int. J. Hydrogen Energy*, 2012, **37**(19), 14265–14277.
16 A. Fujisawa, S. Miura, Y. Mitsutake and M. Monde, Simulation study of hydrogen purification using metal hydride, *J. Alloys Compd.*, 2013, **580**, S423–S426.
17 M. D. Nashchekin, M. V. Minko, S. B. Morgunova and K. B. Minko, Enhancement of heat-and mass-transfer processes in a metal-hydride flow-through hydrogen-purification reactor, *Int. J. Hydrogen Energy*, 2020, **45**(46), 25013–25029.
18 Y. Qin, R. Song, S. Chen, Y. Chen, J. Hou, N. Xu and W. Zhang, First-principles studies on the hydrogen storage

properties of XMoH3 (X= Na, K, Rb, Cs) perovskite hydrides, *Int. J. Hydrogen Energy*, 2024, **88**, 251–259.
19 Y. Liu, H. Du, X. Zhang, Y. Yang, M. Gao and H. Pan, Superior catalytic activity derived from a two-dimensional Ti 3 C 2 precursor towards the hydrogen storage reaction of magnesium hydride, *Chem. Commun.*, 2016, **52**(4), 705–708.
20 S. Zhang, X. Feng, G. Yang and B. Wen, The hardness and electrical conduction in TiB2 and MgB2: Computational insights, *Comput. Mater. Sci.*, 2024, **232**, 112642.
21 T. Sruthi and V. Mathew, Computational investigation of quantum capacitance enhancement in Mg-substituted MgB2-based supercapacitor electrodes, *Comput. Condens. Matter*, 2024, **40**, e00940.
22 H.-W. Li, Y. Yan, S.-i. Orimo, A. Züttel and C. M. Jensen, Recent progress in metal borohydrides for hydrogen storage, *Energies*, 2011, **4**(1), 185–214.
23 E. Beheshti, A. Nojeh and P. Servati, A first-principles study of calcium-decorated, boron-doped graphene for high capacity hydrogen storage, *Carbon*, 2011, **49**(5), 1561–1567.
24 R. K. Sahoo, B. Chakraborty and S. Sahu, Reversible hydrogen storage on alkali metal (Li and Na) decorated C20 fullerene: a density functional study, *Int. J. Hydrogen Energy*, 2021, **46**(80), 40251–40261.
25 M. I. Khan, A. Saeed, M. Shakil, G. Saira, A. Ahmad, F. Imam and S. S. Alarfaji, Computational exploration of high-capacity hydrogen storage in alkali metal-decorated MgB2 material, *J. Power Sources*, 2024, **613**, 234881.
26 M. I. Khan, M. Khurshid, S. S. Alarfaji and A. Majid, Bismuthene as a novel anode material of magnesium/zinc ion batteries with high capacity and stability: a DFT calculation, *Phys. Chem. Chem. Phys.*, 2024, **26**(42), 27007–27018.
27 M. I. Khan, G. Nadeem, A. Majid and M. Shakil, A DFT study of bismuthene as anode material for alkali-metal (Li/Na/K)-ion batteries, *Mater. Sci. Eng. B*, 2021, **266**, 115061.
28 M. I. Khan, A. Majid, N. Ashraf and I. Ullah, A DFT study on a borophene/boron nitride interface for its application as an electrode, *Phys. Chem. Chem. Phys.*, 2020, **22**(6), 3304–3313.
29 M. I. Khan, I. Mehmood, S. S. Alarfaji, M. Junaid and T. Iqbal, Computational study of novel 2H chromium ditelluride as an anode material for Li/K-ion batteries, *RSC Adv.*, 2024, **14**(47), 34515–34525.
30 M. I. Khan, M. Anwar, A. Majid, M. Shakil and M. Rizwan, Computational studies of super-B as anodes for AM (Li, Na, and K) ion batteries, *J. Electrochem. Soc.*, 2022, **169**(9), 090514.
31 M. I. Khan, S. Aslam, A. Majid and S. S. A. Gillani, Intercalation of Lithium inside bilayer buckled borophene: a first principles prospective, *J. Electrochem. Soc.*, 2021, **168**(7), 070535.
32 G. Te Velde, F. Bickelhaupt, E. Baerends, C. Fonseca Guerra, S. Van Gisbergen, J. G. snijders and t. ziegler, Chemistry with ADF, *J. Comput. Chem.*, 2001, **22**(9), 931–967.
33 S. Grimme, J. Antony, S. Ehrlich and H. Krieg, A consistent and accurate ab initio parametrization of density functional dispersion correction (DFT-D) for the 94 elements H-Pu, *J. Chem. Phys.*, 2010, **132**(15), 154104.
34 F. Fan, J. Ren, Y. He and X. Chen, DFT study of Mg decorated on the planar B2N as a novel hydrogen storage media, *Results Phys.*, 2023, **46**, 106263.
35 R. Varunaa and P. Ravindran, Potential hydrogen storage materials from metal decorated 2D-C 2 N: an ab initio study, *Phys. Chem. Chem. Phys.*, 2019, **21**(45), 25311–25322.
36 Z. Liu, P. Wang, Q. Cui, G. Yang, S. Jin and K. Xiong, Theoretical prediction of HfB 2 monolayer, a two-dimensional Dirac cone material with remarkable Fermi velocity, *RSC Adv.*, 2019, **9**(5), 2740–2745.
37 L. Zhang, Z. Wang, S. Du, H.-J. Gao and F. Liu, Prediction of a Dirac state in monolayer TiB 2, *Phys. Rev. B*, 2014, **90**(16), 161402.
38 M. Wan, S. Zhao, Z. Zhang and N. Zhou, Two-dimensional BeB2 and MgB2 as high capacity Dirac anodes for Li-ion batteries: A DFT study, *J. Phys. Chem. C*, 2022, **126**(23), 9642–9651.
39 H. Zhang, Y. Li, J. Hou, A. Du and Z. Chen, Dirac state in the FeB2 monolayer with graphene-like boron sheet, *Nano Lett.*, 2016, **16**(10), 6124–6129.
40 B. Chettri, P. Patra, N. N. Hieu and D. Rai, Hexagonal boron nitride (h-BN) nanosheet as a potential hydrogen adsorption material: A density functional theory (DFT) study, *Surf. Interfaces*, 2021, **24**, 101043.
41 G. Saira, S. M. Zaigam, M. I. Khan, M. B. Tahir, M. Rafique and S. S. Alarfaji, Computational study of Be/Mg-decorated hexagonal chromium ditelluride (CrTe2) for hydrogen storage applications, *J. Energy Storage*, 2024, **103**, 114221.
42 I. López-Corral, E. Germán, A. Juan, M. A. Volpe and G. P. Brizuela, DFT study of hydrogen adsorption on palladium decorated graphene, *J. Phys. Chem. C*, 2011, **115**(10), 4315–4323.
43 I. K. Petrushenko and K. B. Petrushenko, Hydrogen adsorption on graphene, hexagonal boron nitride, and graphene-like boron nitride-carbon heterostructures: A comparative theoretical study, *Int. J. Hydrogen Energy*, 2018, **43**(2), 801–808.
44 A. N. Sosa, B. J. Cid, Á. Miranda, L. A. Pérez, G. H. Cocoletzi and M. Cruz-Irisson, A DFT investigation: high-capacity hydrogen storage in metal-decorated doped germanene, *J. Energy Storage*, 2023, **73**, 108913.
45 B. Silvi and A. Savin, Classification of chemical bonds based on topological analysis of electron localization functions, *Nature*, 1994, **371**(6499), 683–686.
46 C. S. Abraham, S. Muthu, J. C. Prasana, S. Armaković, S. J. Armaković and B. Geoffrey, Computational evaluation of the reactivity and pharmaceutical potential of an organic amine: A DFT, molecular dynamics simulations and molecular docking approach, *Spectrochim. Acta, Part A*, 2019, **222**, 117188.
47 M. Vatanparast and A.-R. Nekoei, RAHB concept and σ-skeleton in some oximes of 3-hydroxy fulvene; DFT, AIM, ELF and NBO studies, *Struct. Chem.*, 2015, **26**, 1039–1048.
48 M. I. Khan, M. I. Akber, M. Gul, T. Iqbal, S. S. Alarfaji and A. Mahmood, Exploring the sensing potential of Fe-decorated h-BN toward harmful gases: a DFT study, *RSC Adv.*, 2024, **14**(10), 7040–7051.